

# TIME-DOMAIN FILTERING FOR SPATIAL LARGE-EDDY SIMULATION

C. David Pruett\*

Department of Mathematics

James Madison University

Harrisonburg, Virginia 22807 USA

540-568-6227 (T) 540-568-6857 (F) dpruett@math.jmu.edu

1997 ASME Fluids Engineering Division Summer Meeting

FEDSM'97 June 22-26, 1997

FEDSM97-3117

## ABSTRACT

An approach to large-eddy simulation (LES) is developed whose subgrid-scale model incorporates filtering in the time domain, in contrast to conventional approaches, which exploit spatial filtering. The method is demonstrated in the simulation of a heated, compressible, axisymmetric jet, and results are compared with those obtained from fully resolved direct numerical simulation. The present approach was, in fact, motivated by the jet-flow problem and the desire to manipulate the flow by localized (point) sources for the purposes of noise suppression. Time-domain filtering appears to be more consistent with the modeling of point sources; moreover, time-domain filtering may resolve some fundamental inconsistencies associated with conventional space-filtered LES approaches.

## 1 INTRODUCTION

By definition, direct numerical simulation (DNS) is the numerical solution of the Navier-Stokes equations without recourse to empirical models. In concept, the fluid motions are resolved down to the Kolmogorov length scale, at which eddies succumb to viscous dissipation. Consequently, for high Reynolds number flow, the computational requirements of fully resolved DNS are staggering.

In contrast, in large-eddy simulation (LES), the large scales of motion are resolved in space and time on a suitable computational grid; however, the effects of the subgrid-scale motions on the evolution of the large scales are modeled. Relative to DNS, LES is conducted on relatively coarse grids at reasonable computational expense. In practice, LES involves filtering the Navier-Stokes equations in space or time or both. The filtered equations of motion contain subgrid-scale (residual) stress terms whose effects must be modeled.

Both DNS and LES can be classified fundamentally as temporally or spatially evolving. The distinction between tem-

poral and spatial approaches is muddied by most applications of LES. In particular, nearly all current LES approaches, whether temporal or spatial, exploit spatial filtering. In their review paper, Moin and Jimenez (1993) state: "Historically, temporal filtering has not been used," one presumes for reasons of computational efficiency. However, because the roles of space and time are fundamentally interchanged in temporal vs. spatial simulations, we suggest that spatial filtering is more appropriate for temporal LES, and conversely, temporal filtering is more appropriate for spatial LES. Indeed, time-domain filtering may remove some of the conceptual and practical inconsistencies that have been observed by practitioners of LES, a few of which are discussed briefly below.

First, as intimated by Germano (1992), LES can be viewed as lying somewhere near the middle of a spectrum of numerical solution techniques with DNS at one end and Reynolds-averaged Navier-Stokes (RANS) at the other end. In our opinion, this point of view is most self-consistent if time-domain filtering is exploited in LES as it is in RANS. Second, Moin and Jimenez (1993) observe that the operations of filtering and differentiation do not commute on a non-uniform mesh. Consequently, most subgrid-scale models inadvertently impose different levels of dissipation in different regions of the computational domain, a problem made worse on the highly stretched grids associated with complicated geometries. This problem should be circumvented by temporal filtering in conjunction with uniform time increments. Third, again according to Moin and Jimenez (1993): "In LES, it is highly desirable for the filter width to be significantly larger than the computational mesh to separate the numerical and modeling errors. Practical considerations, however, usually require the filter width and mesh to be of the same order. In this case, there does not appear to be a necessity for higher than second order numerical methods for LES." In contrast, for the present temporally filtered approach, the filter width is typically an order of magnitude larger than the time step. Fourth, it may be desirable in spatial DNS or LES of certain physical problems (e.g., jet flow) to allow for time-dependent localized (point) sources as a means of manipulating the flow for the purposes of control. For example, such sources could be used to introduce local disturbances to enhance or inhibit mixing. Dakhoul and Bedford (1986) suggest that spatial filtering is fundamentally inconsistent with the introduction of point sources, whereas temporal filtering of a point source is

\*Research conducted under NASA Grant NAS1-1802, monitored by Dr. Kristine R. Meadows, NASA Langley Research Center, Hampton, VA 23681-0001

well defined.

Whereas Dakhoul and Bedford (1986) and Aldama (1990) propose and develop space-time filters for LES, the author is unaware of any purely time-filtered approach. In the next few sections, we develop and demonstrate a spatial LES concept based on filtering in the time domain, and we apply the approach to the investigation of large coherent structures (CS) in a heated subsonic axisymmetric jet. For several reasons, the jet-flow problem is well suited to the particular LES approach. First, free shear layers, jets, and wakes, whose mean streamwise velocity profiles are inflectional, are inviscidly unstable to disturbances of a broad spectrum of frequencies (wavelengths). As a consequence, DNS of three-dimensional (3D) unbounded shear flows is presently impractical because of the extremely fine grid resolution required, and some sort of subgrid-scale dissipation is virtually a necessity. Second, the problem is of immediate practical interest to the field of computational aeroacoustics (CAA). Specifically, it is generally believed that, for supersonic jets, most of the noise originates from the CS rather than from the small-scale turbulence (Seiner, 1984, and Tam, 1995). For subsonic jets, the origin of noise is less certain. In his recent review paper, Tam (1995) expresses the view that subsonic jet noise originates primarily from fine-scale turbulence. Our results (preliminary at the present time) would suggest otherwise. Thus, spatial LES may provide a tool by which to investigate the physics of noise production and suppression in jets. Last, because no walls are present, we avoid for the time being the difficulties experienced by many subgrid-scale models in the vicinity of solid boundaries.

In the next section, time-domain filtering is discussed in general, and a prototype causal digital filter is developed. The governing equations for DNS are discussed in Section 3, and the equations are modified for LES based on adaptation of the so-called SEZHu ("says who") model of Speziale and coworkers (1988). The present model differs from the SEZHu model in that it exploits temporal rather than spatial filtering. The axisymmetric-jet test case is defined in Section 4. The numerical approach to the solution of the governing equations, adapted from Pruett et al. (1995), is addressed briefly in Section 5. Results of LES for the axisymmetric-jet problem are presented in Section 6 and are compared with well-resolved DNS results. Finally, some brief conclusions are offered in Section 7.

## 2 CAUSAL FILTERING

Time-domain filters fall into either of two categories: causal or acausal. For application to LES, only causal filtering is realizable. By definition, causal temporal filters exploit present and past information only, the future being inaccessible. Consequently, in this section, we consider prototypical continuous and discrete causal filters. A continuous filter is presented for conceptual purposes; an analogous discrete filter is exploited in practice.

**A CONTINUOUS CAUSAL FILTER:** If  $s(t)$  represents a smooth continuous signal in time  $t$ , then a continuous low-pass causal filter can be constructed simply by integrating the signal over the interval  $\Delta$ , the temporal window width, as follows:

$$\bar{s}(t, \Delta) = \frac{1}{\Delta} \int_{t-\Delta}^t s(\tau) d\tau \quad (1)$$

The input to Eq. 1 is the raw signal  $s(t)$ , and the output is the continuous filtered signal, denoted by  $\bar{s}(t, \Delta)$ . From elementary calculus, the following property of the filter defined by Eq. 1 is readily derived:

$$\bar{s}(t, 0) \equiv \lim_{\Delta \rightarrow 0} \bar{s}(t, \Delta) = s(t) \quad (2)$$

In general,  $\bar{\bar{s}} \neq \bar{s}$  If  $\Delta$  represents some moderately large temporal window, then filtering  $s(t)$  via Eq. 1 will tend to remove oscillations of high frequency relative to  $\Delta$  while preserving low-frequency oscillations, which defines a "low-pass" time-domain filter.

**LINEAR DIGITAL CAUSAL FILTERS:** Let us digitize the continuous signal  $s(t)$  such that  $s_i = s(t_i)$ , where  $t_i = i\Delta t$ , and  $\Delta t$  is the (constant) time interval between samples. Typically, for applications to LES,  $\Delta$  should be an order of magnitude larger than  $\Delta t$ . The approximation of Eq. 1 by a linear quadrature rule results in its discrete analog

$$\bar{s}_i = \sum_{j=0}^m p_j s_{i-j} \quad (3)$$

where the filter coefficients  $p_j$  are determined to give the filter certain desirable properties (e.g., low-pass characteristics, stability, and high-order accuracy at low frequencies). Following Press et al. (1986), we generalize the linear digital filter given in Eq. 3 to allow the use of previously filtered data. Specifically, suppose

$$\bar{s}_i = \sum_{j=0}^m p_j s_{i-j} + \sum_{k=1}^n q_k \bar{s}_{i-k} \quad (4)$$

The filter of Eq. 4 is "nonrecursive" if  $q_k = 0$  for all  $k$  and "recursive" if, for at least one  $k$ ,  $q_k \neq 0$ , in which case the current value of the filtered quantity is a linear combination of previous unfiltered and filtered values.

**FREQUENCY RESPONSE:** It is instructive to examine the frequency response of the filter associated with Eq. 4. From Press et al. (1986), the transfer function, which quantifies the frequency response, is given by

$$H(\Omega) = \frac{\sum_{j=0}^m p_j e^{-i\Omega j}}{1 - \sum_{k=1}^n q_k e^{-i\Omega k}} \quad (5)$$

where  $i = \sqrt{-1}$ ,  $\Omega = \omega^* \Delta t^*$  is the dimensionless frequency,  $\omega^* = 2\pi f^*$  is the dimensional circular frequency, and  $f^*$  is the dimensional physical frequency. (Throughout this work, we denote dimensional quantities by asterisks.) In general, the frequency response of a recursive filter is related to a rational polynomial function in the complex variable  $1/\zeta$ , where  $\zeta = e^{i\Omega}$ . Thus, recursive filters are to nonrecursive filters what compact-difference operators are to standard finite-difference operators. The rational polynomial form of the transfer function allows considerable latitude in shaping the frequency response. Fig. 7 compares the modulus of the transfer function of a prototypical low-pass digital recursive filter with that of an idealized "spectral cutoff" filter, for a nominal cutoff frequency  $\Omega'_c$ . Note that, for the spectral cutoff filter,  $\bar{\bar{s}} = \bar{s}$ , which, as we have mentioned previously, is not true in general. The transfer function of the digital filter can be made to more closely approximate the spectral ideal at the expense

of including more and more history (i.e., by using larger and larger values of  $m$  and  $n$ .)

For the purposes of time-filtered LES, the design constraints for the discrete filter are: 1) stability for all  $t$ ; 2)  $H(0) = 1$ ; 3) high-order accuracy; 4)  $|H(\Omega)| = 0$  for  $\Omega > \Omega_c$ ; and 5) as little storage required as possible. For reasons to be addressed fully in a subsequent paper, one is lead to the fortunate if surprising conclusion that second-order filters are optimal for the present application to LES. First, second-order causal filters require relatively little storage for history. Second, to avoid mixing the truncation errors of the filter and numerical method, one should invoke a filter with no higher order than that of the time-advancement scheme. Thus, a second-order filter is compatible with the present third-order time advancement scheme (see Section 5). Third, and a subtle point, it can be shown that second-order filtering is consistent with the underlying subgrid-scale model (Pruett, 1996b). Consequently, for our purposes, we have followed the design procedures outlined in the digital signal filtering text by Strum and Kirk (1988). Formally, our prototype filter is a second-order, impulse-invariant, digital Butterworth low-pass filter, for which  $m = n = 2$ , and  $p_0 = 0$ . Technically, Butterworth filters are "all-pole" filters, whose transfer functions are maximally flat in the vicinity of the origin. Unfortunately, however, the transfer functions of Butterworth filters do not vanish identically for large values of  $\Omega$ . In practice, this is not a problem as will be shown subsequently. The nominal cutoff frequency for our prototype filter is  $\Omega'_c = 1.0$ , for which  $|H(\Omega'_c)|^2 = 0.5$ .

A suitable generalization from the prototype filter to a tunable-cutoff low-pass filter is made by incorporating a parameter  $R_c$ , defined as the ratio of the actual and prototypical cutoff frequencies, namely

$$R_c = \frac{\Omega_c}{\Omega'_c} = \frac{\Delta t}{\Delta} \quad (6)$$

Note that  $R_c \rightarrow 0$  for the discrete filter is analogous to  $\Delta \rightarrow \infty$  for the continuous filter of Eq. 1. Conversely, as  $R_c \rightarrow \infty$ ,  $\Delta \rightarrow 0$ , in which case  $\bar{s}(t, \Delta) \rightarrow s(t)$  by the property of Eq. 2. Fig. 7 shows the frequency response of the present filter for  $R_c = 1.25$ , a value typical for the current time-filtered LES approach. Note that high-frequency oscillations are virtually eliminated by the present filter, as desired.

### 3 GOVERNING EQUATIONS

We first specify the governing equations for DNS and then present the governing system as modified for LES.

**DNS:** As a basis on which to evaluate various LES solutions, we require a well-resolved DNS solution for the axisymmetric-jet problem. For a compressible fluid, it is appropriate to define a fluid state vector  $[\rho, p, T, u, v, w]^T$  comprised of the density  $\rho$ , pressure  $p$ , temperature  $T$  and velocity components  $u, v$ , and  $w$ . The governing equations for the axisymmetric-jet problem are adapted from those presented in Pruett et al. (1995) for a body-fitted coordinate system  $\bar{x} = [x, \theta, z]^T$  on an axisymmetric body, where  $x$  as the arc length along the body,  $\theta$  is the azimuthal angle,  $z$  is the coordinate normal to the body,  $r = R + z \cos \phi$  is the radial coordinate,  $R(x)$  is the body radius, and  $\phi(x)$  is the angle of the surface tangent to the body. For the jet-flow application,  $R = \phi = 0$ , in which

case the coordinate system degenerates to  $z = r$  with  $x$  as the axial coordinate, whereby  $u$  and  $w$  become the axial and radial velocities, respectively. Because  $R = 0$ , the equations are geometrically singular along the jet axis. For the continuity equation, the singularity is removed by applying L'Hopital's rule along the axis ( $z = 0$ ). The singularity is not problematic for the momentum and energy equations because axial boundary conditions replace the governing equations along the axis. Specifically, considerations of symmetry require that the azimuthal velocity ( $v$ ) vanish everywhere and that

$$\frac{\partial T}{\partial z} = \frac{\partial u}{\partial z} = w = 0 \quad (z = 0) \quad (7)$$

**LES AND SUBGRID-SCALE MODEL:** If the compressible Navier-Stokes equations (CNSE) are filtered in the time domain according to Eq. 1, the resulting equation system is formally identical to that of Eqs. (15), (16), and (34) of Erlebacher et al. (1992), where overbars and tildes distinguish conventionally filtered and Favre-filtered quantities, respectively. In general, the use of Favre-filtered (density-weighted) variables reduces the complexity of the filtered CNSE. Specifically, for example, the Favre-filtered axial velocity is defined as

$$\bar{u} = \frac{\overline{\rho u}}{\bar{\rho}} \quad (\text{or } \bar{\rho} \bar{u} = \overline{\rho u}) \quad (8)$$

Other Favre-filtered quantities are defined analogously. For the filtered equations, the fluid state vector is comprised of a mixture of conventionally and Favre-filtered quantities, namely  $[\bar{\rho}, \bar{p}, \bar{T}, \bar{u}, \bar{v}, \bar{w}]^T$ . The filtered governing equations contain residual stresses not present in the original equations, which are decomposed into Leonard-stress, cross-stress, and Reynolds-stress terms denoted by  $L, C$ , and  $R$ , respectively, following the notation of Erlebacher et al. (1992). Of these,  $C$  and  $R$  must be modeled;  $L$  can be computed.

Several candidate subgrid-scale models are available; however, for our present purpose, we adapt the SEZHu model (Speziale et. al, 1988) as adapted by Erlebacher et al. (1992). Several considerations favor this selection. First, to demonstrate the time-filtered approach, the filtering process must participate in the model, rather than simply serving as a conceptual framework as it does in some models (e.g., Smagorinsky). Second, although present results suggest that a dynamic model (Germano et al., 1991) is desirable, we wanted initially to avoid some of the pitfalls of dynamic subgrid-scale models, particularly, the need to smooth the computed model constants. Finally, the SEZHu model is extremely well documented in Erlebacher et al. (1992).

Formally, our implementation of the SEZHu model is virtually identical to that of Erlebacher et al. (1992), except, of course, that the filter is temporal. In tensor notation, the dimensionless filtered equations, with the modeled terms denoted by underlines, are

$$\gamma M^2 \bar{p} = \bar{p} \bar{T} \quad (9)$$

$$\frac{\partial \bar{p}}{\partial t} + \frac{\partial (\bar{p} \bar{u}_k)}{\partial x_k} = 0 \quad (10)$$

$$\frac{\partial (\bar{p} \bar{u}_k)}{\partial t} + \frac{\partial}{\partial x_i} \left[ \bar{p} \bar{u}_k \bar{u}_i + \bar{p} (\bar{u}_k \bar{u}_i - \bar{u}_k \bar{u}_i) \right] = - \frac{\partial \bar{p}}{\partial x_k} + \frac{\partial}{\partial x_i} \left[ (\underline{\mu}_v + \underline{\mu}_T) \bar{S}_{ki} \right] \quad (11)$$

$$\frac{\partial \bar{p}}{\partial t} + \frac{\partial}{\partial x_k} \left[ \bar{p} \bar{u}_k + \frac{\bar{p}}{\gamma M^2} (\bar{u}_k \bar{T} - \bar{u}_k \bar{T}) \right] = -(\gamma - 1) \bar{p} D + \frac{\partial}{\partial x_k} \left[ (\kappa_v + \kappa_T) \frac{\partial \bar{T}}{\partial x_k} \right] + \frac{(\gamma - 1) \Phi}{Re} \quad (12)$$

where

$$D = \frac{\partial \bar{u}_k}{\partial x_k} \quad (13)$$

is the resolved-scale dilatation,

$$\bar{S}_{kl} = 2(\bar{e}_{kl} - \frac{1}{3} D \delta_{kl}) \quad (14)$$

$\delta_{kl}$  is the Kronecker delta, and  $\bar{e}_{kl}$  is the resolved-scale strain-rate tensor, namely

$$\bar{e}_{kl} = \frac{1}{2} \left[ \frac{\partial \bar{u}_k}{\partial x_l} + \frac{\partial \bar{u}_l}{\partial x_k} \right] \quad (15)$$

For brevity, the physical viscosity and thermal conductivity are denoted, respectively, as

$$\mu_v = \frac{\bar{\mu}}{Re} ; \quad \kappa_v = \frac{\bar{\mu}}{M^2 Re Pr} \quad (16)$$

where  $Re$ ,  $Pr$ , and  $M$  are the dimensionless Reynolds, Prandtl, and Mach numbers, respectively. Similarly, the eddy viscosity and the eddy thermal conductivity are given by

$$\mu_T = C_r l^2 \bar{\rho} \Pi^{1/2} ; \quad \kappa_T = \frac{\mu_T}{\gamma M^2 Pr_T} \quad (17)$$

where  $l$  is a length scale to be defined shortly,  $Pr_T$  is the turbulent Prandtl number,  $\gamma$  is the ratio of specific heats, and

$$\Pi = \bar{S}_{kl} \bar{S}_{kl} \quad (18)$$

Whereas the underlined terms on the right-hand sides of the governing equations model  $R$ , the underlined terms on the left-hand sides, which are properly referred to as the resolved stresses, are computable by filtering the resolved fields. For the present subgrid-scale model, the resolved stresses model the sum  $L + C$ .

In the original SEZHu subgrid-scale model (Speziale et al., 1988), the Reynolds stresses were split into deviatoric and isotropic parts, which were modeled separately. In the more detailed paper of Erlebacher et al. (1992), on which the present approach is based, the isotropic part is disregarded on the rationale that its contribution should be small for turbulent Mach numbers  $M_t < 0.6$  (a constraint satisfied by most compressible flows). Several other subtleties of the implementation of the model are not immediately apparent upon the study of Erlebacher et al. (1992). First, the viscous-stress terms of the filtered momentum equations, and the dissipation function  $\Phi$  and thermal-stress terms of the filtered energy equation, formally involve conventionally filtered rather than Favre-filtered quantities. Because these quantities are unavailable, however, they are approximated by their Favre-filtered equivalents. Second, terms that arise from subgrid-scale fluctuations of  $\mu_v$  and  $\kappa_v$  are neglected. Third, the resolved stresses are computed using  $\bar{p}$  rather than  $\rho$ , the latter of which is unavailable. These approximations should be considered as additional modeling errors.

**MODEL CONSTANTS:** Equation 17 requires values for three constants. Following Erlebacher et al. (1992), we use  $Pr_T = 0.5$  and  $C_r = 0.012$ . It remains to determine  $l$ , which, for the original SEZHu model, is a characteristic length scale related to spatial grid resolution. Specifically, Erlebacher et al. (1992) show that  $l = c \Delta x$  is optimal (in the sense of preserving the Galilean invariance of certain terms of the model) for  $c = 2$ , where  $\Delta x$  is the actual computational grid spacing.

Here, we must determine  $l$  based on the choice of the temporal scale  $\Delta$  (or equivalently,  $R_c$ ), for which purposes we appeal to results from the area of hydrodynamic stability. From linear stability theory, we know that jets, wakes, and free shear layers are dispersive; i.e., waves of different frequencies propagate at different phase velocities. However, disturbances of moderate to high frequencies propagate at a velocity approximately that of  $U_{av}^*$ , the average of the jet and ambient velocities. Accordingly, we define  $\Delta x^*$  as the characteristic size of an eddy associated with a disturbance of cutoff frequency  $f_c^*$ ; that is

$$\Delta x^* = \frac{U_{av}^*}{f_c^*} = \frac{2\pi U_{av}^* \Delta t^*}{R_c} \quad (19)$$

Finally, we note that the CNSE are recovered from the governing equations in the limit as  $\Delta \rightarrow 0$ .

## 4 TEST CASE

The numerical test case was chosen to approximately replicate an acoustics experiment that is being conducted at NASA Langley Research Center. Specifically, we investigate a heated subsonic ( $M = 0.8$ ) jet exhausting into a nearly quiescent atmosphere. The jet temperature  $T_j^*$ , on which the Mach number is based, is 600 F (1059.6 R), and the ambient temperature is 70 F (529.6 R). The nominal jet radius is  $R_j^* = 0.5$  in. (0.0417 ft.). The ambient pressure in the physical experiment is approximately one atmosphere (2160 psf.). However, this results in too high a Reynolds number for a DNS computation of reasonable expense; consequently, the computational experiment assumes an ambient pressure 10 percent that of the physical experiment; that is, 216 psf., which results in  $Re = 10153$  based on the jet conditions and the nominal jet radius. In the physical experiment, the ambient air was quiescent. However, computational experiments with unbounded shear layers typically encounter numerical difficulties (as did the present work) whenever the ambient stream is perfectly quiescent (Tannehill et al., 1994). Consequently, it is customary for the jet to exhaust into a coflowing stream with a velocity of a few percent of the jet velocity. For the present problem, we use an ambient to jet velocity ( $U_j^*$ ) ratio of 10 percent. We further assume that the jet is fully expanded, in which case, in the absence of any disturbances, the pressure is constant both radially and axially.

In the governing equations and in the results to follow, all lengths have been normalized by  $R_j^*$ , and the velocities, temperature, and density, have been normalized by  $U_j^*$ ,  $T_j^*$ , and  $\rho_j^*$ , respectively. Pressure is normalized by  $\rho_j^* U_j^{*2}$ .

## 5 NUMERICAL METHODOLOGY

Spatial DNS and LES can be viewed as three-step processes. First, an unperturbed time-independent base state is obtained, usually by boundary-layer techniques. Second, the base state is subjected to either random or temporally periodic perturbations, which are typically imposed at or near the computational inflow boundary. The structure of these disturbances is commonly obtained from linear stability theory, or more recently, from parabolized stability equation (PSE) methodology. Third, the spatial evolution of the propagating disturbances is computed by solution of the complete Navier-Stokes equations, with (LES) or without (DNS) subgrid-scale models. We discuss in turn each of these steps in the context of the current problem.

**COMPUTATION OF THE BASE STATE:** The application of standard fully implicit boundary-layer techniques to the axisymmetric jet revealed an unanticipated computational difficulty; namely, the Jacobian matrix associated with the iteration procedure was extremely ill-conditioned and the iteration did not converge. The computational problem arises from a reversal of sign in the transverse velocity experienced by internal boundary-layer flows such as jets, wakes, and free shear layers. To circumvent this numerical difficulty, a semi-implicit boundary-layer technique was developed, which is documented in Pruett (1996a). The interested reader is referred to this paper for details. Also to avoid numerical difficulties, the internal shear layer is given finite thickness at the lip of the jet. The boundary-layer solution can be viewed as an unstable equilibrium state of the CNSE.

**IMPOSITION OF THE DISTURBANCES:** The nature of instabilities is different for wall-bounded and free-shear flows. Specifically, wall-bounded flows are subject to viscous instabilities, for which typically only a relatively narrow band of frequencies are unstable. In contrast, free-shear layers, jets, and wakes are subject to inviscid instabilities over a broad range of frequencies. Relative to viscous instabilities, inviscid instabilities experience rapid growth rates. Thus, for simulating instability waves in wall-bounded flows, it is essential that the imposed disturbances be consistent with eigenfunctions obtained from stability theory; otherwise, one introduces spatial transients that may corrupt the particular instability of interest. On the other hand, one can be somewhat cavalier in imposing disturbances in free-shear flows because of the flow's tendency to rapidly organize arbitrary disturbances into the dominant eigenmodes. Consequently, following Mankbadi et al. (1994), at the inflow boundary, we impose a temporally periodic fluctuation comprised of a few harmonics of specified frequencies, but whose structure is not derived from stability theory. At present, we impose the disturbance only through the streamwise velocity. Specifically, at the inflow boundary  $x = x_0$

$$u(t, x_0, z) = u_B(x_0, z) + \epsilon u'(t, z) \quad (20)$$

$$u'(t, z) = \phi(z) [\sin(\omega_f t) + \cos(0.5\omega_f t)] \quad (21)$$

$$\phi(z) = \exp[-(2(z-1))^4] \quad (22)$$

where the subscript  $B$  denotes the base state, the prime denotes a fluctuating quantity, and the subscript  $f$  denotes the fundamental frequency. The function  $\phi(z)$  is used to shape the disturbance profile so that the disturbance is largest near the edge of the jet but essentially vanishes along the jet axis and at the far-field boundary. Numerical experimentation reveals the most rapid development of the jet for  $\omega_f = \pi$ , which

corresponds to a Strouhal number ( $St = f_f R_j / U_j^*$ ) of 0.5, in keeping with the observations of Mankbadi et al. (1994). Following the early computational investigation of free-shear layers by Riley and Metcalfe (1980), we include an out-of-phase subharmonic component to enhance pairing of adjacent vortices. At present, we use a forcing amplitude of  $\epsilon = 0.005$ , which is ramped up slowly (over a time interval of one period of oscillation at the fundamental frequency) to minimize temporal transients.

**DNS AND LES METHODOLOGIES:** For both the DNS and LES, we adapt the high-order numerical scheme of Pruett et al. (1995), to which the reader is referred for details. Briefly, this algorithm exploits fully explicit time advancement, high-order compact-difference methods (Lele, 1992) for aperiodic spatial dimensions, and spectral collocation methods for periodic spatial dimensions. Specifically, for the present axisymmetric-jet application, we use fourth- and sixth-order compact difference schemes in the axial and radial dimensions, respectively. The azimuthal dimension, of course, does not come into play for the axisymmetric case. The method of Pruett et al. (1995) uses a variable step for time advancement in the context of a three-stage, low-storage Runge-Kutta (RK3) scheme. However, the present LES application, which involves temporal filtering, requires a constant time step. Consequently, the original Runge-Kutta temporal integration has been replaced by a fixed-length, multiple-step, third-order Adams-Bashforth (AB3) technique. An additional motivation for replacing the RK3 method was that it was not immediately clear to the author how temporal filtering would interact with time advancement whenever multiple stages per time step were involved, the fear being the possibility of numerical instability. The storage requirement for the algorithm with AB3 time advancement is about 150 percent that of the original algorithm with RK3. In general, multiple-step methods are not self starting. The AB3 integration is started initially with a single first-order Euler step followed by one second-order Adams-Bashforth step. Because the perturbation is ramped slowly to full amplitude, and the initial state is in (near) equilibrium, the initial loss of temporal accuracy is inconsequential.

For both the DNS and the LES, the symmetry conditions given by Eq. 7 are imposed along the jet axis. At the inflow boundary, for the present axisymmetric-jet problem, the flow is everywhere subsonic, and one characteristic points upstream. Consequently, not all flow variables can be specified. Currently, we specify  $v$ ,  $w$ ,  $T$ , and the incoming Riemann invariants. At the far-field boundary ( $z = z_{\max}$ ), we adapt the non-reflecting boundary conditions of Thompson (1987) as modified by Pruett et al. (1995). At the outflow boundary, we exploit a buffer-domain approach (Streett and Macaraeg, 1989/1990). Near the outflow boundary, a buffer zone of finite width is constructed in which both the base state and the governing equations are modified to ensure that all waves propagate out of the domain.

Finally, we note that the present LES algorithm is one of few to incorporate high-order numerical methods, another being that of El-Hady and coworkers [5].

**COMPUTATIONAL EFFICIENCY:** On the same grid, an LES computation with the present algorithm requires not quite twice the computational effort as DNS and approximately 2.5 times the storage for 3D flows (twice the storage for two-dimensional or axisymmetric flows). Most of the additional memory is relegated to storage of the time histo-

ries of quantities associated with the time-filtered approach. One must keep in mind, however, that, by definition, LES allows computations on coarser grids than DNS. If, for the present LES algorithm, for example, the grid resolution relative to DNS could be reduced by a factor of three in each of the three spatial dimensions and time, then storage requirements would be diminished by a factor of approximately ten, and processor time would diminish by a factor of approximately 40. Thus, measures of efficiency in LES must consider not only nominal storage and operation counts, but also the potential grid-coarsening factor, which could conceivably be higher for temporally filtered LES than for conventional approaches.

## 6 RESULTS

For the DNS and LES results presented below, the computational domain was

$$0 \leq x \leq 20 \quad ; \quad 0 \leq z \leq 5 \quad (23)$$

The length of the domain was sufficient to allow one pairing of the adjacent vortices shed at the edge of the jet. The final 16 percent of the axial extent of the domain lies in the buffer domain; results within the buffer domain should be disregarded as unphysical. For convenience in presenting results, we define  $t_P$ , the time in periods of oscillation at the fundamental disturbance frequency.

**DNS:** The DNS results were obtained on the computational domain defined above at an extremely fine spatial grid resolution of  $1280 \times 512$  and a temporal resolution of 2048 steps per (fundamental) disturbance period. To arrive at this resolution, computations were made on successively finer grids beginning from a coarse grid of  $256 \times 128$ . For each spatial resolution, an estimate of the temporal resolution necessary for stability was made based on stability analyses of model advection and diffusion equations. All computations except for that on the finest grid eventually "blew up" due to numerical instabilities associated with unresolved scales. In contrast, Fig. 7 shows instantaneous contours of constant density at  $t_P = 18$  for the fully resolved computation. On the finest grid, the DNS computation required in excess of 20 CPU hours on a Cray C90. Consequently, calculations at a higher Reynolds number would have been impractical given the computational resources available.

The present fine-grid DNS represents one of the most accurate and highly refined computations of an unbounded shear layer of which we are aware, another being that of Colonius et al. (1995), and Fig. 7 affords considerable detail. It is interesting to note a striking correlation between the contours of constant density and those of constant vorticity (not shown due to space limitations). Both quantities clearly show the roll-up of the shear layer at the jet's edge into a vortex street and the subsequent pairing of adjacent vortices, phenomena common to unbounded shear flows. A similar comparison of vorticity and pressure contours is also most revealing. Not unexpectedly, the centers of low pressure correspond precisely with the centers of the large vortices. As adjacent vortices merge, the individual pressure lows are replaced by larger and stronger low pressure regions. High pressure regions lie between adjacent vortices.

**LES:** For LES of jet flow, the trick is to find an appropriate amount of eddy viscosity. If the LES subgrid-scale

model is insufficiently dissipative, the computation will blow up. On the other hand, if the model is excessively dissipative, the instabilities that result in vortex shedding and pairing are suppressed or diminished. It appears possible, however, that an intermediate amount of dissipation will preserve the large-scale features of the flow while preventing numerical instabilities associated with unresolved scales. In particular, Figs. 7 and 7 present instantaneous contours of constant density and pressure, respectively, obtained from an LES computation with a spatial grid resolution of  $432 \times 192$ , coarser by a factor of approximately three in each direction than the DNS computation presented previously. The time is  $t_P = 18$ , and the temporal resolution is 1024 time steps per period. Because fully explicit time-advancement schemes typically yield over-resolution in time, practicality demands a filter width  $\Delta$  that is approximately, say, an order of magnitude larger than the time step. Here, we used  $\Delta/\Delta t = 8$  ( $R_c = 0.125$ ). At this cutoff frequency, the maximum eddy viscosity was approximately eight times the maximum physical viscosity. Whereas the DNS calculation required 20 CPU hours, the  $432 \times 192$  LES calculation required two CPU hours. (Calculations on the coarsest grid of  $256 \times 128$ , for which the computation eventually blew up, required only a matter of minutes.) Relative to the DNS results of Fig. 7, the shear-layer roll-up and pairing events of the moderately dissipative LES computation are retarded, but not prevented. Consequently, we believe the moderately resolved LES could serve as a computational platform for the investigation of jet noise. To this end and following Colonius et al. [3], we extract the compressible dilatation from the numerical solution; The instantaneous dilatation field at  $t_P = 18$  of the moderately resolved LES computation is shown in Fig. 7. It would appear that, in terms of the dilatation, each large vortex appears as an acoustic quadrupole. These results suggest that significant acoustic radiation is associated with the large-scale vortices, in contrast to the view expressed by Tam (1995) for subsonic jets.

For the present work in progress, our primary objective has been to demonstrate the feasibility and practicality of time-filtered spatial LES. As one possible measure of success, we examine the resolved subgrid-scale stresses computed by the time-filtered subgrid-scale model, the principal component of which is presented in Fig. 7. For an LES computation, the magnitude of the resolved stresses can be viewed as a measure of ill resolution, or equivalently, as identifying the regions where additional dissipation is needed to prevent numerical instability. For the present time-filtered approach, these terms are well defined, judging by the apparent smoothness of the contours in the figure. In summary, these results suggest that a time-filtered dynamic subgrid-scale model could be developed. We suspect that dynamic modeling (Germano et al., 1991) would improve the present results by limiting the eddy viscosity only to regions where it is needed. For this reason, the dynamic approach is judged to be more appropriate for transitional flows, as was demonstrated for compressible flow, for example, in the work of El-Hady et al. (1993).

In closing, we comment that computations of 2D or axisymmetric unbounded shear flows are both less and more difficult than computations of 3D flows. Although the total computational requirements are lower for simulations in 2D, the resolution needed for those two dimensions may well be greater than for the same two dimensions of a 3D simulation. The reason is that, in 3D, the third dimension provides a path for relief of Reynolds stresses that cannot be relieved in 2D. Complete validation of the present time-filtered LES concept

and its application to aeroacoustics ultimately will require the consideration of fully 3D flows.

## 7 CONCLUSIONS

- Time-domain filtering for the residual-stress models of LES is a viable concept that should be investigated further. Preliminary results suggest that time-domain filtering may have significant advantages relative to conventional space-filtered approaches.
- The current baseline LES algorithm is one of a very few LES algorithms to exploit high-order numerical methods.
- The present subgrid-scale model, which involves time-domain filtering, might be improved for application to transitional flows by recasting it in a dynamic-model context (Germano et al., 1991).
- The present approach to LES appears to be applicable to aeroacoustics, as had been hoped.
- A thorough validation of the time-filtered LES approach and its usefulness to aeroacoustics will require LES of fully 3D flows.

## ACKNOWLEDGEMENTS

In addition to the financial support of NASA Langley Research Center acknowledged on page 1, the computational support of the National Aerodynamic Simulator (NAS) at NASA Ames Research Center is also gratefully acknowledged. The author is also indebted to Drs. Gordon Erlebacher, Ugo Piomelli, and Klaus Adams for helpful discussions and clarifying insights.

## References

- [1] A. A. Aldama, *Filtering Techniques for Turbulent Flow Simulation*, Springer-Verlag, Berlin, 1990.
- [2] D. A. Anderson, J. C. Tannehill, and R. H. Pletcher, *Computational Fluid Mechanics and Heat Transfer*, Hemisphere Publishing Company, 1984, pp. 391-394.
- [3] T. Colonius, S. K. Lele, and P. Moin, "The Sound Generated by a Two-Dimensional Shear Layer: A Comparison of Direct Computations and Acoustic Analogies," CEAS/AIAA Paper No. 95-036.
- [4] Y. M. Dakhoul and K. W. Bedford, "Improved Averaging Method for Turbulent Flow Simulation. Part I: Theoretical Development and Application to Burgers' Transport Equation," *Int. J. Num. Meth. Fluids*, Vol. 6, 1986, pp. 49-64.
- [5] N.M. El-Hady, T.A. Zang, and U. Piomelli, "Dynamic Subgrid-Scale Modeling for High-Speed Transitional Boundary Layers," in *Engineering Applications of Large Eddy Simulations-1993*, eds. S.A. Ragab and U. Piomelli, FED-Vol. 1962, 1993, pp. 103-112.
- [6] G. Erlebacher, M. Y. Hussaini, C. G. Speziale, and T. A. Zang, "Toward the Large-Eddy Simulation of Compressible Turbulent Flows," *J. Fluid Mech.*, Vol. 238, 1992, pp. 155-185.
- [7] M. Germano, "Turbulence: The Filtering Approach," *J. Fluid Mech.*, Vol. 238, 1992, pp. 325-336.
- [8] M. Germano, U. Piomelli, P. Moin, and W. H. Cabot, "A Dynamic Subgrid-Scale Eddy Viscosity Model," *Phys. Fluids A*, Vol. 3, 1991, pp. 1760-1765.
- [9] S. K. Lele, "Compact Finite Difference Schemes with Spectral-Like Resolution," *J. Comput. Phys.*, Vol. 103, 1992, pp. 16-42.
- [10] P. Moin and J. Jimenez, "Large-Eddy Simulation of Complex Turbulent Flows," AIAA Paper No. 93-3099, 1993.
- [11] R. R. Mankbadi, M. E. Hayder, and L. A. Povinelli, "Structure of Supersonic Jet Flow and Its Radiated Sound," *AIAA J.*, Vol. 32, No. 5, 1994, pp. 897-906.
- [12] W. H. Press, B. P. Flannery, S. A. Teukolsky, and W. T. Vetterling, *Numerical Recipes: The Art of Scientific Computing*, Cambridge University Press, Cambridge, 1986, pp. 436-444.
- [13] C. D. Pruett, "A Semi-Implicit Method for Internal Boundary-Layer Flows," *Comp. Meth. Applied Mech. Eng.*, 1996, (to appear).
- [14] C. D. Pruett, "Toward the Simplification of Dynamic Subgrid-Scale Models," paper submitted for the First AFOSR International Conference on Direct Numerical Simulation and Large-Eddy Simulation, to be held at Louisiana Tech Univ., Ruson, LA, Aug. 4-8, 1997.
- [15] C. D. Pruett, T. A. Zang, C.-L. Chang, and M. H. Carpenter, "Spatial Direct Numerical Simulation of High-Speed Boundary-Layer Flows-Part I: Algorithmic Considerations and Validation," *Theoret. Comput. Fluid Dynamics*, Vol. 7, No. 5, 1995, pp. 49-76.
- [16] J. J. Riley and R. W. Metcalfe, "Direct Numerical Simulation of a Perturbed, Turbulent Mixing Layer," AIAA Paper No. 80-0274, 1980.
- [17] J.M. Seiner, "Advances in High-Speed Jet Aeroacoustics," AIAA Paper No. 84-2275, 1984.
- [18] C. G. Speziale, G. Erlebacher, T. A. Zang, and M. Y. Hussaini, "The Subgrid-Scale Modeling of Compressible Turbulence," *Phys. Fluids A*, Vol. 31, No. 4, 1988, pp. 940-942.
- [19] C. L. Streett and M. G. Macaraeg, "Spectral Multi-Domain for Large-Scale Fluid Dynamic Simulations," *App. Numer. Math.*, Vol. 6, 1989/1990 pp. 123-139.
- [20] R. D. Strum and D. E. Kirk, *First Principles of Discrete Systems and Digital Signal Processing*, Addison-Wesley, New York, 1988.
- [21] C. R. Tam, "Supersonic Jet Noise," *Annu. Rev. Fluid Mech.*, Vol. 27, 1995, pp. 17-43.
- [22] K. W. Thompson, "Time Dependent Boundary Conditions for Hyperbolic Systems," *J. Comput. Phys.*, Vol. 68, 1987, pp. 1-24.

## FIGURES

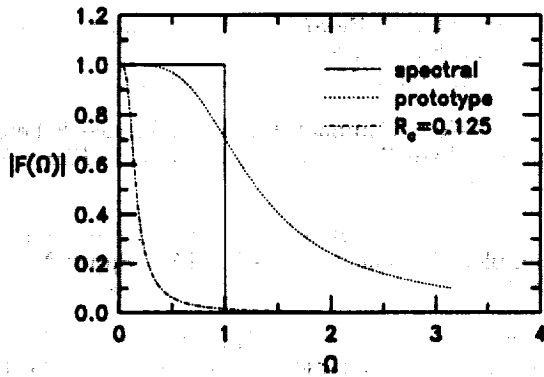


Figure 1. Transfer function of prototype second-order causal filter compared with spectral-cutoff transfer function.

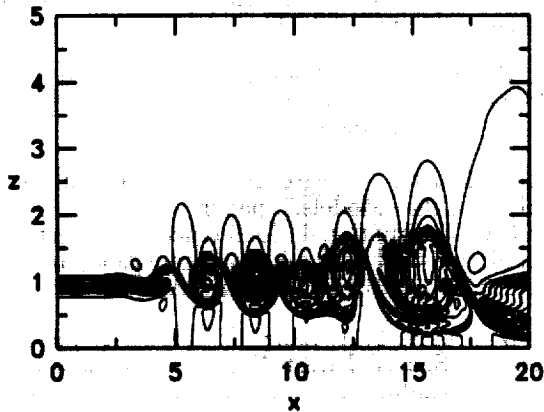


Figure 2. Contours of constant density obtained from well-resolved ( $1280 \times 512$ ) DNS calculation at  $t_P = 18$ . Flow is left to right. Jet centerline is along lower boundary of figure. Contour levels denote variations of  $0.82 \leq \rho \leq 2.15$ . Buffer domain shown.

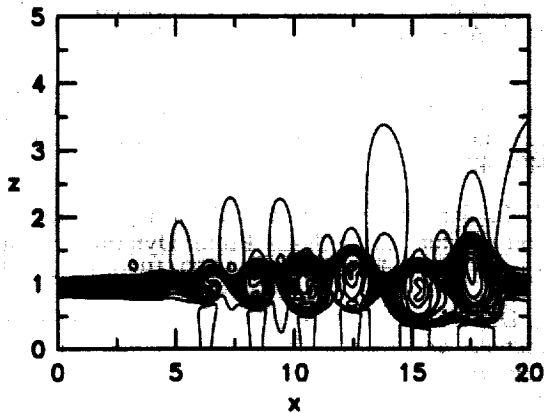


Figure 3. Contours of constant density obtained at  $t_P = 18$  from LES of  $432 \times 192$  grid resolution. Maximum eddy viscosity is 8 times that of physical viscosity. Relative to DNS, vortex roll-up and pairing events are retarded but not prevented. Contour levels denote variations of  $0.95 \leq \rho \leq 2.13$ . Buffer domain shown.

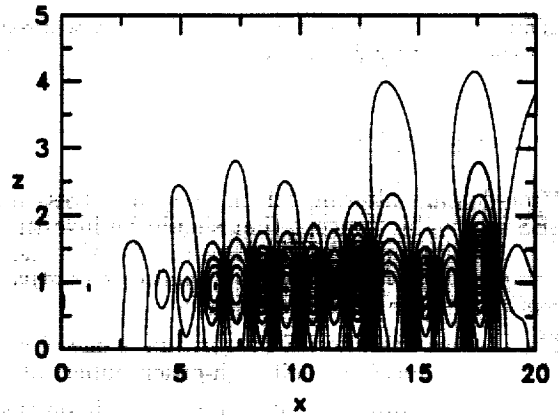


Figure 4. Contours of constant pressure obtained from LES calculation of resolution  $432 \times 192$  at  $t_P = 18$ . Contour levels denote variations of  $0.87 \leq p \leq 1.26$ . Buffer domain shown.

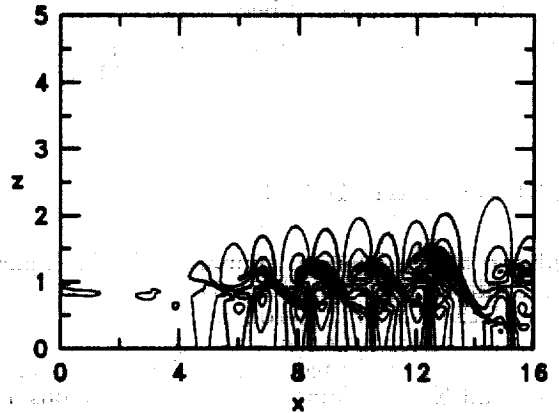


Figure 5. Isolevels of dilatation  $D$  obtained at  $t_P = 18$  from LES of  $432 \times 192$  grid resolution. Contour levels denote variations of  $-0.10 \leq D \leq 0.13$ . Buffer domain not shown.

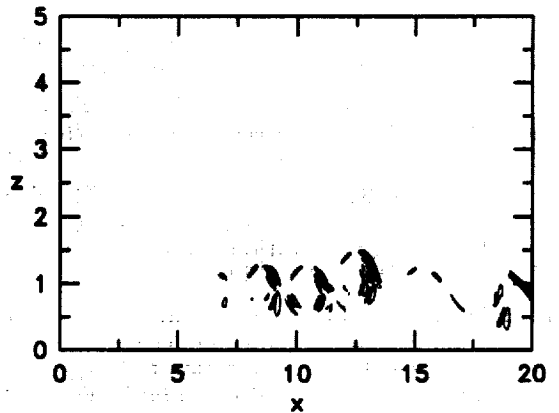


Figure 6. Principal component of resolved stresses obtained at  $t_P = 18$  from LES of  $432 \times 192$  grid resolution. Contour levels denote variations from  $-4.2 \times 10^{-5}$  to  $3.3 \times 10^{-5}$ . Buffer domain shown.